Spectra of magnetic fields from electroweak symmetry breaking

Tanmay Vachaspati[1] and Axel Brandenburg[2,3,4,5]

[1]*Physics Department, Arizona State University, Tempe, Arizona 85287, USA*
[2]*Nordita, KTH Royal Institute of Technology and Stockholm University, 10691 Stockholm, Sweden*
[3]*The Oskar Klein Centre, Department of Astronomy, Stockholm University, 10691 Stockholm, Sweden*
[4]*School of Natural Sciences and Medicine, Ilia State University, 0194 Tbilisi, Georgia*
[5]*McWilliams Center for Cosmology and Department of Physics, Carnegie Mellon University, Pittsburgh, Pennsylvania 15213, USA*

(Received 10 December 2024; accepted 3 February 2025; published 24 February 2025)

We characterize magnetic fields produced during electroweak symmetry breaking by nondynamical numerical simulations based on the Kibble mechanism. The generated magnetic fields were thought to have an energy spectrum $\propto k^3$ for small wave numbers k, but here we show that it is actually a spectrum $\propto k^4$ along with characteristic fluctuations in the magnetic helicity. Using scaling results from magnetohydrodynamics simulations for the evolution and assuming that the initial magnetic field is coherent on the electroweak Hubble scale, we estimate the magnetic field strength to be $\sim 10^{-13}$ G on kpc scales at the present epoch for nonhelical fields. For maximally helical fields we obtain $\sim 10^{-10}$ G on Mpc scales. We also give scalings of these estimates for partially helical fields.

DOI: 10.1103/PhysRevD.111.043541

I. INTRODUCTION

The standard model of particle physics implies that electroweak symmetry breaking in the universe occurred at a temperature ~ 100 GeV and at a cosmic time $\sim 10^{-10}$ s when the horizon size was ~ 1 cm. It is not clear if the dynamics of electroweak symmetry breaking occurs as a first- or second-order phase transition or as a crossover, as this is sensitive to new ingredients present in particle physics (dark matter, generation scheme for neutrino masses, etc.). What is certain, however, is that the Higgs field responsible for electroweak symmetry breaking acquires a nonvanishing vacuum expectation value (VEV). It has been argued that the very process of the Higgs acquiring a VEV generates a primordial magnetic field [1], and simulations of electroweak symmetry breaking by a few different groups [2–4] show that a few percent of the cosmic energy density at the electroweak epoch is in the form of magnetic fields (see the reviews [5–9]).

Once electroweak symmetry has been broken in the universe, further evolution of the magnetic field obeys Maxwell's equations in the presence of the cosmic plasma. We expect the evolution to be well described by the equations of magnetohydrodynamics (MHD). However, the initial conditions for MHD evolution have to be derived from electroweak physics. Key features of the initial conditions are the energy and helicity spectra of the magnetic fields. One approach to obtaining such initial conditions is to evolve the electroweak equations through the process of electroweak symmetry breaking [2–4]. These field theory simulations are computationally expensive, and their limited dynamical range cannot resolve the spectral slope at small wave numbers with a sufficient degree of certainty.

In this paper we take a different approach to determine the spectra of magnetic fields generated during electroweak symmetry breaking. The key idea is the "Kibble mechanism," also employed in studying the formation of topological defects [10,11]. The germ of the idea is that the Higgs VEV will be spatially (and temporally) varying during electroweak symmetry breaking. Then, topological considerations, as discussed below, necessarily imply the presence of magnetic charges and, hence, magnetic fields. After electroweak symmetry breaking has completed, the magnetic charges will have annihilated but the magnetic field will survive. It is this magnetic field that we wish to characterize. An advantage of using the Kibble mechanism is that it is not limited by dynamical range; a disadvantage is that it does not take into account any dynamics except for those dictated by symmetry considerations.

The calculation of magnetic fields resulting from the Kibble mechanism is subtle because the algorithm necessarily produces magnetic monopoles connected by Z-strings, also known as "Nambu dumbbells" [12,13]. A straightforward calculation of the magnetic field, $\mathbf{B}$, will not satisfy $\mathrm{div}\mathbf{B} = 0$ and MHD evolution, as it assumes the absence of magnetic charges would not apply. Instead we want to construct the divergence-free magnetic field that results after the magnetic monopoles have annihilated and the Nambu dumbbells have dissipated. We devise a novel algorithm to construct the magnetic field, essentially by mimicking the

eventual conversion of the Z-string to the electromagnetic magnetic field, as seen in Ref. [14].

We start in Sec. II by defining the electromagnetic field strength in terms of electroweak variables. The topological aspects of the standard model are outlined, together with the reason for the existence of magnetic monopoles. In Sec. III we discuss the electroweak magnetic monopole explicitly. This explicit monopole configuration is useful for testing the numerical algorithm described in Sec. IV. An important feature of our numerical algorithm is that it takes into account the Z-strings that, when converted into electromagnetic fields, are necessary to ensure the divergence-free condition. The results of our numerical analysis are described in Sec. V. In this section we also use current results on MHD evolution to estimate the cosmological magnetic field at the present epoch. We conclude in Sec. VI. In Appendix A we outline an alternate algorithm to evaluate the magnetic field, one which accurately reproduces the monopole configuration but is somewhat less convenient to implement in the Pencil Code [15] that we use. In Appendix B we revisit and correct the analytical estimate in Ref. [9] to obtain the k^4 energy spectrum. In Appendix C we relate some of our scaling exponents to the symbols used earlier in the literature.

II. ELECTROWEAK SYMMETRY BREAKING AND ELECTROMAGNETISM

In the standard electroweak model, the electromagnetic (as opposed to the Z-magnetic) magnetic field is given by [1]

$$\mathbf{B} = \nabla \times \mathcal{A} - i\frac{2\sin\theta_w}{g\eta^2}\nabla\Phi^\dagger \times \nabla\Phi, \tag{1}$$

where $\mathcal{A}$ is the electromagnetic gauge field, Φ is the vacuum expectation value (VEV) of the Higgs field, $|\Phi| = \eta = 246$ GeV, and $\sin^2\theta_w = 0.23$ and $g = 0.65$ are coupling constants in the model. The last term in (1) requires that the electromagnetic field strength should be gauge invariant under electroweak symmetry transformations and should reduce to the usual Maxwellian definition in "unitary gauge," in which Φ is constant.

The Higgs field is a complex doublet

$$\Phi = \eta\begin{pmatrix}\phi_1 + i\phi_2 \\ \phi_3 + i\phi_4\end{pmatrix} \tag{2}$$

and the Higgs potential is

$$V(\Phi) = \frac{\lambda}{4}(|\Phi|^2 - \eta^2)^2. \tag{3}$$

The vacuum manifold—the minimum of the potential—is given by

$$|\Phi|^2 = \phi_1^2 + \phi_2^2 + \phi_3^2 + \phi_4^2 = \eta^2 \tag{4}$$

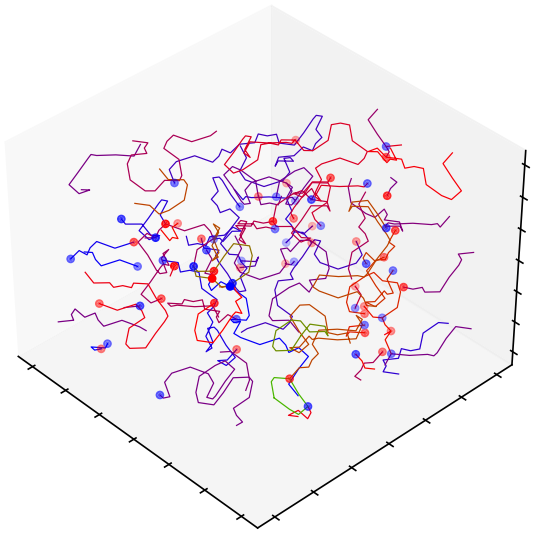

FIG. 1. Distribution of monopoles and antimonopoles and the strings connecting them (from Ref. [13]).

and this describes a three sphere, S^3. Symmetry dictates that the VEV of the Higgs can take on any value on this S^3 with equal probability [10]. The VEVs in distant spatial regions will be independent of each other, implying that $\nabla\Phi$ must be nonzero during electroweak symmetry breaking and, from (1), magnetic fields must be created [1].

A more in-depth analysis reveals the topology in electroweak symmetry breaking [13,16]. Random orientations of Φ imply that the unit vector

$$\hat{n}^a = \frac{\Phi^\dagger\sigma^a\Phi}{\eta^2} \tag{5}$$

will also be distributed randomly. The distribution of a three-vector field can be topologically nontrivial, implying the existence of Higgs zeros and magnetic charges [17,18]. (The "magnetic charge" will be referred to as a "magnetic monopole," though it should be noted that there is no static magnetic monopole solution of the electroweak equations.) Further analysis shows that the electroweak magnetic monopole is connected by a Z-string to an antimonopole and the Higgs field vanishes along the string (see Fig. 1) [12,19]. The dynamics of a monopole-antimonopole pair shows that the system is unstable to decay and that the Z-string converts into an electromagnetic magnetic field [14]. The final magnetic field, after all the monopoles have annihilated, is divergenceless. We would like to determine the spectral properties of the final magnetic field on large length scales.

III. MAGNETIC MONOPOLES

The magnetic field in (1) has two pieces: the first term is divergence-free, while the last term can have nonvanishing divergence and represents the magnetic monopole

contribution. We will be interested in the spectral properties of the latter contribution to the final magnetic field, as it is insensitive to the detailed dynamics of electroweak symmetry breaking. Then the magnetic field is given by

$$\mathbf{B} = -i\frac{2\sin\theta_w}{g\eta^2}\nabla\Phi^\dagger \times \nabla\Phi \tag{6}$$

and the corresponding gauge field using $\mathbf{B} = \nabla \times \mathbf{A}$ is[1]

$$\mathbf{A} = -i\frac{2\sin\theta_w}{g\eta^2}\Phi^\dagger\nabla\Phi, \tag{7}$$

where we have used $\nabla \times \nabla\Phi = 0$. As we shall see below, the gauge field defined in (7) may be multivalued at certain points, and it will be important to handle these singular points carefully.

It is helpful to consider a specific configuration that corresponds to an electroweak magnetic monopole. The Higgs field for the monopole can be written in spherical coordinates as

$$\Phi_m = \eta\begin{pmatrix}\cos(\theta/2)\\ \sin(\theta/2)e^{i\phi}\end{pmatrix}, \tag{8}$$

for which the vector in (5) is

$$\hat{n} = (\sin\theta\cos\phi, \sin\theta\sin\phi, \cos\theta) = \hat{r}. \tag{9}$$

Then the magnetic field derived from (6) is

$$\mathbf{B} = \frac{\sin\theta_w}{g}\frac{\hat{r}}{r^2}, \tag{10}$$

which is the magnetic field of a magnetic monopole. The corresponding gauge field is

$$\mathbf{A} = \frac{\sin\theta_w}{g}\frac{(1-\cos\theta)}{r\sin\theta}\hat{\phi}, \tag{11}$$

where $\hat{\phi}$ is the unit vector in the azimuthal direction. This is the gauge field of a magnetic monopole with a Dirac string at $\theta = \pi$, where $\mathbf{A}$ is multivalued. In the full electroweak model, $|\Phi|$ vanishes along the Dirac string, which gets replaced by a regular field configuration called a Z-string. The Z-string carries Z-magnetic flux but no electromagnetic magnetic flux. However, the Z-string is unstable and rapidly decays by conversion into electromagnetic flux [14]. During this process the magnetic monopoles annihilate and the magnetic field becomes divergenceless.

One way to study magnetic field production during electroweak symmetry breaking is to numerically evolve the dynamical electroweak equations, keeping track of the magnetic field [2–4]. However, such field theory simulations are computationally expensive and their dynamical range is limited. Recognizing that the monopole contribution to the magnetic field arises simply due to variations of the Higgs field, it is more efficient to perform a nondynamical evaluation of the magnetic field, though taking care to account for both the magnetic field of the magnetic monopoles and also the Z-strings that will eventually convert to electromagnetic magnetic fields. We describe the algorithm for the nondynamical evaluation in the next section.

IV. ALGORITHM

The magnitude of the Higgs field is fixed on the vacuum manifold: $|\Phi| = \eta$. The direction of the Higgs field varies on a certain length scale that is determined by the dynamics of electroweak symmetry breaking, as in a first- or second-order phase transition, or a crossover. Then we imagine spatial domains within which the direction of the Higgs is approximately constant, while the Higgs directions in different domains are completely uncorrelated. More concretely, we consider the Hopf parametrization of the Higgs field on its vacuum manifold,

$$\Phi = \begin{pmatrix}\cos\alpha e^{i\beta}\\ \sin\alpha e^{i\gamma}\end{pmatrix}, \tag{12}$$

where $\alpha \in [0, \pi/2]$ and $\beta, \gamma \in [0, 2\pi]$ are Hopf angles on the three sphere given by (4). Electroweak symmetry implies that the probability for α, β, and γ to take on any value is given by the volume element $du d\beta d\gamma$, where $u = \cos(2\alpha)/2$. Therefore, $u \in [-1/2, 1/2]$, $\beta \in [0, 2\pi]$, and $\gamma \in [0, 2\pi]$ are uniformly distributed in their respective domains.

We simulate the distribution of the Higgs field on a cubic lattice, where each cell of the lattice is considered to be a domain of constant Higgs—the lattice spacing corresponds to the domain size. Equivalently, we assign a value of the Hopf angles to each vertex of a cubic lattice by randomly selecting values from their probability distributions. The angles at any vertex define the Higgs field Φ at that vertex by (12).

In our numerical implementation, the zeros of the Higgs field—that are also the locations of the monopoles and Z-strings—fall between lattice points, and hence $\mathbf{A}$ is well defined everywhere on the lattice. From $\mathbf{A}$ we find $\mathbf{B}$, not by taking the curl of $\mathbf{A}$, say by using finite differences, but by calculating fluxes through plaquettes of the simulation lattice,

$$\mathbf{B}\delta x^2 = \hat{p}\oint_{\partial P}\mathbf{dl}\cdot\mathbf{A}, \tag{13}$$

where ∂P denotes the perimeter of the plaquette, and we have assumed that $\mathbf{B}$ is spread uniformly over the area δx^2

[1] $\mathbf{A}$ should not be confused with $\mathcal{A}$ that occurs in (1).

of the plaquette and is oriented along the areal vector $\hat{p}$ of the plaquette (defined by the direction—clockwise or counterclockwise—in which we perform the line integral). The advantage of using (13) is that it automatically includes the contributions of the magnetic monopoles and the strings. (In the electroweak model the strings are Z-strings that decay into electromagnetic magnetic fields; in electromagnetism, the strings are Dirac strings.) The magnetic field that we obtain in this way will be divergenceless because the magnetic monopole contribution to the magnetic field is compensated exactly by the string contribution. We have tested our algorithm to make sure that the string flux is -2π so as to exactly cancel the $+2\pi$ flux of the magnetic monopole.

A simple procedure to evaluate Eq. (13) is given by summing the components of $\mathbf{A}$, defined by (7), along the links of each plaquette between its four vertices, I, II, III, and IV. Starting at the lower left corner and going in the clockwise direction, the contribution between vertices I and II yields

$$A_x|_a = -i\frac{2\sin\theta_w}{g\eta^2}\Phi^\dagger\partial_x\Phi|_a \approx -i\frac{\sin\theta_w}{g\eta^2\delta x}(\Phi_{\rm II}^\dagger+\Phi_{\rm I}^\dagger)(\Phi_{\rm II}-\Phi_{\rm I}), \tag{14}$$

where δx is the lattice spacing. Given that $\Phi_{\rm II}^\dagger\Phi_{\rm II}=\eta^2$ and $\Phi_{\rm I}^\dagger\Phi_{\rm I}=\eta^2$, we are left with

$$A_x|_a \approx -i\frac{\sin\theta_w}{g\eta^2\delta x}\left(\Phi_{\rm I}^\dagger\Phi_{\rm II}-\Phi_{\rm II}^\dagger\Phi_{\rm I}\right) = \frac{2\sin\theta_w}{g\eta^2\delta x}{\rm Im}\Phi_{\rm I}^\dagger\Phi_{\rm II}. \tag{15}$$

In this way, we obtain from all four contributions

$$\oint_{\partial P}\mathbf{dl}\cdot\mathbf{A}\approx\frac{2\sin\theta_w}{g\eta^2}{\rm Im}\big(\Phi_{\rm I}^\dagger\Phi_{\rm II}+\Phi_{\rm II}^\dagger\Phi_{\rm III}+\Phi_{\rm III}^\dagger\Phi_{\rm IV}+\Phi_{\rm IV}^\dagger\Phi_{\rm I}\big). \tag{16}$$

We have checked that this algorithm gives the string flux of -2π so that it exactly cancels the $+2\pi$ flux of the magnetic monopole at sufficiently high resolution. It also agrees with an alternate algorithm presented in Appendix A. For convenience, we will work in units such that $2\sin\theta_w/g=1$ and $\eta=1$.

The above procedure evaluates the magnetic field flux through each plaquette of the lattice, namely $B_x(i,j+1/2,k+1/2)$, $B_y(i+1/2,j,k+1/2)$, and $B_z(i+1/2,j+1/2,k)$ for all vertices (i,j,k). Each component can be Fourier transformed using

$$\mathbf{b}(\mathbf{k})=\int d^3x\mathbf{B}(\mathbf{x})e^{+i\mathbf{k}\cdot\mathbf{x}}. \tag{17}$$

A translation of the coordinate system only introduces an overall phase factor that does not enter the energy spectrum. For example, for the z-component of the magnetic field we can shift the coordinate system by $(1/2,1/2,0)$, resulting in a magnetic field defined on a regular grid, which can be Fourier transformed using a fast Fourier transform routine. The shift introduces an overall phase factor $\exp(i\mathbf{k}\cdot\mathbf{a})$ in the Fourier transform, where $\mathbf{a}$ is the shift vector, but this factor does not affect the energy spectrum, which only depends on $|\mathbf{b}(\mathbf{k})|^2$. Further, the different components of the magnetic field enter the power spectrum independently and can be evaluated using different suitable shifts.

The magnetic field generated by the random distribution of Φ will be isotropic, homogeneous, and divergenceless, and the two-point correlation function will take the standard form, $\langle b_i(\mathbf{k})b_j^*(\mathbf{k}')\rangle=(2\pi)^6\delta^{(3)}(\mathbf{k}-\mathbf{k}')M_{ij}(\mathbf{k})$, given by just two functions of the wave number k,

$$M_{ij}(\mathbf{k})=\frac{E_M(k)}{4\pi k^2}p_{ij}+i\epsilon_{ijk}k^l\frac{H_M(k)}{8\pi k^2}, \tag{18}$$

where $p_{ij}=\delta_{ij}-\hat{k}_i\hat{k}_j$ is the projection operator that ensures the divergenceless condition. The function $E_M(k)$ is called the energy spectrum, and $H_M(k)$ is the helicity spectrum. The energy spectrum is evaluated using

$$E_M(k)(2\pi)^3\delta^{(3)}(0)=\frac{k^2}{(2\pi)^2}\langle|b_i(\mathbf{k})|^2\rangle. \tag{19}$$

On the discrete lattice, the $(2\pi)^3\delta^{(3)}(0)$ on the left-hand side is replaced by V, the lattice volume. Note that the form of the correlation function in (18) only applies to divergenceless magnetic fields, that is after the magnetic monopoles and connecting Z-strings have annihilated.

The scheme described above to find the magnetic field is inadequate to evaluate the magnetic helicity $\mathbf{A}\cdot\mathbf{B}$, as it only provides the gauge field component along the link at the link midpoint, and only the magnetic field component orthogonal to the plaquette and at the center of the plaquette. We would like to obtain all components of the magnetic field at a point, say the vertices of the lattice. To do so, we interpolate the magnetic field from four adjoining plaquettes, as illustrated in Fig. 2. Once we have the magnetic field on the vertices of the lattice, we Fourier transform to get $\tilde{\mathbf{b}}(\mathbf{k})$, where the tilde denotes that this is the interpolated magnetic field. Then the gauge field Fourier coefficients are found using

$$\tilde{\mathbf{a}}(\mathbf{k})=-i\frac{\mathbf{k}}{k^2}\times\tilde{\mathbf{b}}(\mathbf{k}) \tag{20}$$

up to additive terms proportional to $\mathbf{k}$ that are omitted by our gauge choice.

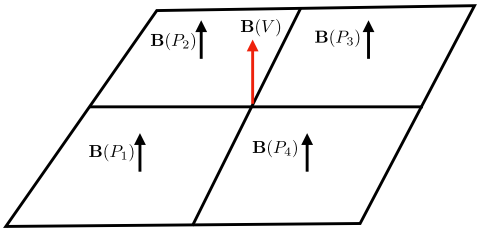

FIG. 2. The z-component of the magnetic field at vertex V is determined by averaging the magnetic field components on the adjoining plaquettes: $B_z(V) = (B_z(P_1) + B_z(P_2) + B_z(P_3) + B_z(P_4))/4$, where the four plaquettes $P_1, \ldots, P_4$ are in the xy-plane.

The helicity spectrum is now evaluated using

$$H_M(k)(2\pi)^3\delta^{(3)}(0) = \frac{k^2}{(2\pi)^2}\langle \tilde{\mathbf{a}}(\mathbf{k}) \cdot \tilde{\mathbf{b}}^*(\mathbf{k})\rangle. \quad (21)$$

Since there is no parity violation present in the Higgs sector of the standard electroweak model,[2] we will have $H_M(k) = 0$ and only helicity fluctuations will be present. Hence, we will also evaluate the shell-integrated helicity variance spectrum,

$$\mathrm{Sp}(h) = \frac{k^2}{8\pi^3 V}\oint d\Omega_k |\tilde{h}|^2, \quad (22)$$

where $h = \mathbf{A} \cdot \mathbf{B}$, $\tilde{h}$ is its Fourier transform, and the integration is over solid angles in k-space. The "Hosking integral," defined as

$$I_H = \frac{2\pi^2}{k^2}\mathrm{Sp}(h)|_{k\to 0}, \quad (23)$$

is a conserved quantity in MHD evolution [20,21]. Its gauge invariance has been proven in Ref. [20] and demonstrated numerically in Ref. [22]. As shown in those earlier papers, the decay of nonhelical MHD turbulence is governed by the conservation of I_H, while the decay of helical MHD turbulence is governed by the conservation of the mean magnetic helicity density $I_M \equiv \langle h \rangle$.

V. RESULTS

A. Spectral scaling at large scales

We compute spectra from a three-dimensional mesh of size L^3, so the smallest wave number in the domain is $k_1 = 2\pi/L$. We use N^3 meshpoints, so the mesh spacing is $\delta x = L/N$, and the largest wave number in the domain is the Nyquist wave number $k_{\mathrm{Ny}} = 2/\delta x = k_1 N/2$.

[2]Parity violation in the electroweak fermionic sector may play a role in producing magnetic helicity but that is not accounted for in the present model.

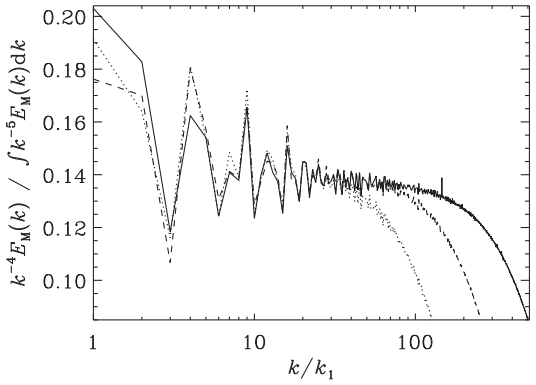

FIG. 3. Compensated magnetic energy spectra, $k^{-4}E_M(k)$, for 256^3 (dotted line), 512^3 (dashed line), and 1024^3 meshpoints (solid line), obtained by using Eq. (16). All curves have been normalized by the value of $\int k^{-5}E_M(k)dk$ for the highest-resolution case.

Our results for the energy spectrum are derived using (19) and shown in Fig. 3, compensated by k^{-4} to show that, at large length scales, it gives the scaling

$$E_M(k) \propto k^4. \quad (24)$$

The exponent disagrees with the analytic argument in [9] where the scaling was estimated to be k^3. In Appendix B we clarify and correct that argument to also show consistency with the numerical scaling of k^4. In Fig. 3, the turnover at large k is due to the discretization error associated with the estimate of the derivative in Eq. (14) for finite mesh spacing and shifts to higher k when N is increased.

To obtain an estimate for the energy spectrum and not just the scaling, we need some input from dynamical simulations [2–4]. The first input is that the energy density in magnetic fields after symmetry breaking is roughly 10% of the total energy density. The second input is that the spectrum in dynamical simulations is highly peaked at the largest coherence scales in the simulations and suggests that the initial coherence scale should be comparable to the cosmological horizon size at the electroweak scale. Even if the coherence scale is initially subhorizon, it will grow on the eddy turnover timescale, which is given by the coherence scale divided by the Alfvén speed, and will be short compared to the Hubble time. This can lead to significant growth of the initial coherence scale, as discussed in [23]. Using the connection between energy density and the energy spectrum,

$$\rho_B = \int dk E_M(k), \quad (25)$$

we get an estimate for the magnetic energy spectrum immediately after electroweak symmetry breaking,

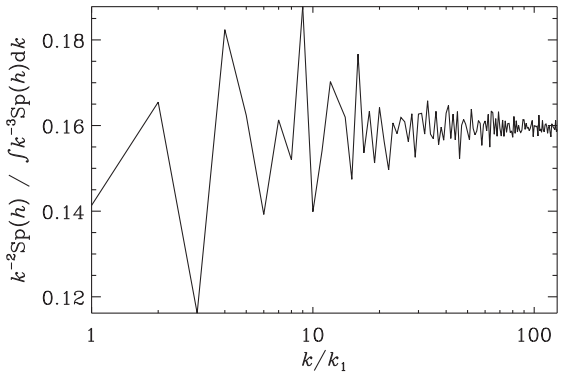

FIG. 4. Compensated shell-integrated helicity variance spectrum, $k^{-2}\mathrm{Sp}(h)$, using $N = 256$ meshpoints, normalized by the value of $\int k^{-3}\mathrm{Sp}(h)dk$.

$$E_M(k, t_{\rm EW}) \sim \frac{\rho_{\rm EW}}{k_{\rm EW}} \left(\frac{k}{k_{\rm EW}}\right)^4, \qquad k < k_{\rm EW}, \tag{26}$$

where $\rho_{\rm EW} \sim (100\ \mathrm{GeV})^4 \sim (10^{24}\ \mathrm{G})^2$ is the energy density at the electroweak scale, and $2\pi/k_{\rm EW} \sim 1$ cm is the physical horizon size at the electroweak epoch.

We do not expect any net magnetic helicity in our simulations, as there is no source of parity violation and $H_M(k) = 0$. In Fig. 4 we plot the k^{-2} compensated shell-integrated helicity variance spectrum and find it to be approximately constant on all scales. Similarly to the normalization employed in the compensated spectrum in Fig. 3, we have normalized the compensated spectrum $k^{-2}\mathrm{Sp}(h)$ by $\int k^{-3}\mathrm{Sp}(h)dk$.

B. Inverse cascade scaling

To estimate the magnetic field predicted from electroweak symmetry breaking at the present epoch we shall assume that the initial coherence scale is given by the cosmological horizon size and has a k^s spectrum for small k. We will give estimates for general s. Our numerical estimates for the location and amplitude of the peak of the spectrum will turn out to be independent of the initial slope of the subinertial ($k < k_{\rm peak}$) range, though other predictions can be sensitive to the actual value of s.

As time evolves, for the nonhelical case the peak of the energy spectrum moves to lower k, as given by the k^ϵ ($\epsilon = 3/2$) envelope in Fig. 5, and the spectrum grows as τ^γ, where τ is conformal time, with [24,25]

$$\gamma = \frac{2(s-\epsilon)}{\epsilon+3} \tag{27}$$

for small k, as follows from the scaling arguments of Ref. [24] and confirmed by the inset of Fig. 5 for $s = 4$ when $\gamma = 10/9$ (see Appendix C for a conversion of the symbols used here to those used in earlier literature—the symbol γ used above is not to be confused with the Hopf angle that is denoted by the same symbol). We wish to

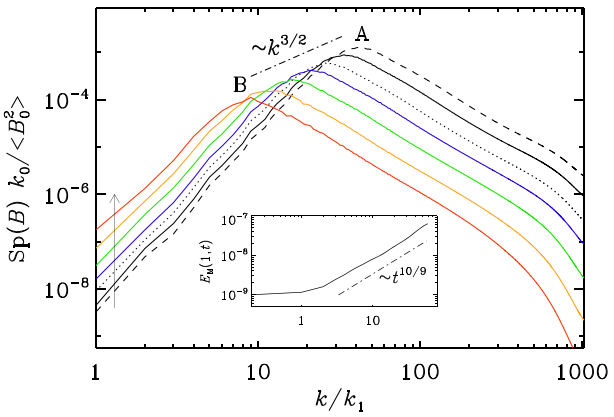

FIG. 5. $E_M(k, t)$ vs k for different times from MHD evolution of an initial k^4 spectrum with vanishing helicity. Point A is the peak location at the initial time and point B is the peak location at the final time. The decay of the peak from A to B follows a $k^{3/2}$ envelope. The vertical arrow and the inset show growth of the power $\propto t^{10/9}$ on small k.

relate the peak of the spectrum at the present epoch τ_0 (labeled as point B in Fig. 5) to the peak of the spectrum at the electroweak epoch $\tau_{\rm EW}$ (labeled as point A). From the k^ϵ envelope we find

$$E_M(k_B, \tau_0) = E_M(k_A, \tau_{\rm EW}) \left(\frac{k_B}{k_A}\right)^\epsilon, \tag{28}$$

and using the k^s spectrum and the τ^γ growth we also find

$$E_M(k_B, \tau_0) = E_M(k_A, \tau_{\rm EW}) \left(\frac{k_B}{k_A}\right)^s \left(\frac{\tau_0}{\tau_{\rm EW}}\right)^\gamma. \tag{29}$$

Note that the evolution is in terms of comoving quantities, for example, $k = ak^{\rm phys}$ and $B = a^2 B^{\rm phys}$, where a is the cosmic scale factor. Also note that the scaling laws used above are only valid at late times, which we assume is given by $\tau \gg \tau_{\rm EW}$, when transients have died out (see Sec. V D).

Dividing (28) by (29) and using (27) we get

$$k_B = k_A \left(\frac{\tau_{\rm EW}}{\tau_0}\right)^{2/(\epsilon+3)}. \tag{30}$$

Inserting this relation into (28) gives,

$$E_M(k_B, \tau_0) = E_M(k_A, \tau_{\rm EW}) \left(\frac{\tau_{\rm EW}}{\tau_0}\right)^{2\epsilon/(\epsilon+3)}. \tag{31}$$

The spectral slope s does not appear in these relations, except for the constraint that $s > \epsilon$.

The conformal magnetic field on scale $\lambda = 2\pi/k$ is given by $\mathcal{B}_\lambda(\tau) = \sqrt{2kE_M(k,\tau)}$, and the physical magnetic field is the conformal magnetic field multiplied by T^2, where T is the cosmic temperature. Therefore, the physical peak magnetic field today is

$$B_B^{\rm phys}(t_0) = B_A^{\rm phys}(\tau_{\rm EW})\left(\frac{\tau_{\rm EW}}{\tau_0}\right)^p \left(\frac{T_0}{T_{\rm EW}}\right)^2, \quad (32)$$

where $p = (\epsilon+1)/(\epsilon+3)$, and the "phys" superscript denotes physical, not comoving, quantities. The peak magnetic field strength at the electroweak epoch is $B_A^{\rm phys}(\tau_{\rm EW}) \sim 10^{24}$ G.

The conformal time is given by $\tau \propto 1/T$ in the radiation dominated universe (for $T \gtrsim T_{\rm eq} \sim 1$ eV) and $\tau \propto 1/\sqrt{T}$ in the matter dominated universe. (We ignore the changes in the number of degrees of freedom and other cosmological events for these simple estimates.) The electroweak temperature is $T_{\rm EW} \sim 100$ GeV and the temperature at the present epoch is $T_0 \sim 10^{-4}$ eV. These numbers give

$$\frac{\tau_0}{\tau_{\rm EW}} = \frac{T_{\rm EW}}{T_{\rm eq}}\sqrt{\frac{T_{\rm eq}}{T_0}} \approx 10^{13}. \quad (33)$$

For nonhelical fields, when $I_H = {\rm const}$, we have $\epsilon = 3/2$, and (30) and (32), with $p = 5/9$, give [26]

$$k_B^{\rm phys} \sim (1\ {\rm kpc})^{-1}, \qquad B_{\rm kpc}^{\rm phys}(t_0) \sim 10^{-13}\ {\rm G}. \quad (34)$$

These estimates are independent of the slope of the spectrum s, which will only enter the estimate of the field strength on length scales other than the peak length scale by factors of $(k/k_B)^s$.

Our formulae in (30) and (32) can also be applied to the case of maximally helical magnetic fields, when $I_M = {\rm const}$. Then $\epsilon = 0$ because E_M at the peak stays constant for maximally helical fields. These numerical values give $p = 1/3$ [see below (32)], and the estimates are

$$k_B^{\rm phys} \sim (1\ {\rm Mpc})^{-1}, \qquad B_{\rm Mpc}^{\rm phys}(t_0) \sim 10^{-10}\ {\rm G}, \quad (35)$$

independent of the spectral slope s.

C. Partially helical decay

The magnetic fields generated during EWSB are expected to be partially helical [23,27,28]. How does partial helicity affect the evolution of the magnetic field and our estimates? With partial helicity, the evolution in the early stages is as if there was no helicity. Then E_M follows Fig. 5 and $\epsilon = 3/2$. However, kH_M is conserved and the field evolves toward maximal helicity, which is defined by $|H_M|_{\rm max} = 2E_M/k$. Once the field is maximally helical, it evolves with $\epsilon = 0$.

Let us denote the conformal time at which the field becomes maximally helical by τ_*. Then applying (30) and (31) from $\tau_{\rm EW}$ to τ_* with $\epsilon = 3/2$, and then from τ_* to τ_0 with $\epsilon = 0$, gives

$$k_B = k_A\left(\frac{\tau_{\rm EW}}{\tau_*}\right)^{4/9}\left(\frac{\tau_*}{\tau_0}\right)^{2/3}, \quad (36)$$

$$E_M(k_B,\tau_0) = E_M(k_A,\tau_{\rm EW})\left(\frac{\tau_{\rm EW}}{\tau_*}\right)^{2/3}. \quad (37)$$

To estimate τ_*, we first define the relative helicity,

$$r_h(k,\tau) = \frac{k|H_M|}{2E_M}. \quad (38)$$

While r_h is a function of k and τ in general, the most relevant value of r_h is at the peak of the spectrum, and we will only consider the relative helicity at the peak scale $k = k_{\rm peak}$. Then τ_* is defined by $r_h(\tau_*) = 1$. Using (37) and the conservation of magnetic helicity gives

$$\tau_* = \tau_{\rm EW} r_{h,\rm EW}^{-3/2}, \quad (39)$$

where $r_{h,\rm EW}$ is the helicity fraction at the electroweak epoch.

The magnetic field becomes maximally helical prior to the present epoch if $\tau_* < \tau_0$, that is, if $r_{h,\rm EW} > (\tau_{\rm EW}/\tau_0)^{2/3} \sim 10^{-9}$. If, on the other hand, $r_{h,\rm EW} < 10^{-9}$, then there is not enough time for the field to become maximally helical and the evolution is just as in the case of nonhelical fields, as in (34). If $r_{h,\rm EW} > 10^{-9}$, Eqs. (36) and (37) with (39) give

$$k_B = k_A r_{h,\rm EW}^{-1/3}\left(\frac{\tau_{\rm EW}}{\tau_0}\right)^{2/3}, \quad (40)$$

$$E_M(k_B,\tau_0) = E_M(k_A,\tau_{\rm EW}) r_{h,\rm EW}, \quad (41)$$

which give the numerical estimates

$$k_B^{\rm phys} \sim (1\ {\rm Mpc})^{-1} r_{h,\rm EW}^{-1/3}, \qquad B_B^{\rm phys}(t_0) \sim 10^{-10} r_{h,\rm EW}^{1/3}\ {\rm G}. \quad (42)$$

D. Relation to earlier decay laws

The scalings (30) and (32) are equivalent to earlier ones in terms of length scales $\xi_M(\tau) \equiv k_B^{-1}$ and mean magnetic energy densities $\mathcal{E}_M(\tau) \equiv B_B^2(\tau)/2$ (see, e.g., Refs. [25,29]). Such relations were typically written in the form

$$\xi(\tau) = \xi(\tau_i)[1 + (\tau-\tau_i)/\tau_{\rm eddy}]^{2/(\epsilon+3)}, \quad (43)$$

$$\mathcal{E}(\tau) = \mathcal{E}(\tau_i)[1 + (\tau-\tau_i)/\tau_{\rm eddy}]^{-2p}, \quad (44)$$

where $\tau_{\rm eddy}$ is some relevant eddy turnover time. Different variations of these expressions have in common that the late-time behavior ($\tau \to \infty$) can be written as

$$\xi(\tau) = \left[\xi(\tau_i)/\tau_{\rm eddy}^{2/(\epsilon+3)}\right]\tau^{2/(\epsilon+3)}, \tag{45}$$

$$\mathcal{E}(\tau) = \left[\mathcal{E}(\tau_i)\tau_{\rm eddy}^{2p}\right]\tau^{-2p}. \tag{46}$$

In the case when I_H is conserved with $2/(\epsilon+3) = 4/9$ and $2p = 10/9$, this can also be written as

$$\xi(\tau) = C_\xi^H I_H^{1/9}\tau^{2/(\epsilon+3)}, \tag{47}$$

$$\mathcal{E}(\tau) = C_\mathcal{E}^H I_H^{2/9}\tau^{-2p}. \tag{48}$$

Conversely, when I_M is conserved with $2/(\epsilon+3) = 2/3 = 2p = 2/3$, these relations can also be written as

$$\xi(\tau) = C_\xi^M I_M^{1/3}\tau^{2/(\epsilon+3)}, \tag{49}$$

$$\mathcal{E}(\tau) = C_\mathcal{E}^M I_M^{2/3}\tau^{-2p}. \tag{50}$$

This may look like a useless introduction of new parameters, but the important point here is that I_H and I_M are conserved quantities and the coefficients C_i^j for $i = \xi$ or $\mathcal{E}$ and $j = H$ or M are believed to be universal ones. The coefficients are known from earlier work and are independent of the initial conditions, while I_H and I_M depend on the initial conditions but do not change during the subsequent evolution. Thus, in reality, there are no free adjustable parameters in this expression anymore.

E. Relevance of the prefactors

Although the scalings (30) and (32) strictly apply to late times, they can be extended to arbitrary times, but we must ensure that the starting values, k_A and B_A, are physically meaningful. This requires that the time since the beginning of the decay is at all times a certain fraction C_M of the Alfvén time, $\tau_{\rm A} = \xi/v_A$, where $v_A = (2\mathcal{E}/\rho)^{1/2}$ is the Alfvén speed [30]. One may, therefore, expect $\tau_{\rm A} = C_M(\tau - \tau_i)$. However, as discussed in Ref. [21], the correct counting of time is uncertain, particularly at early times, and becomes more certain only at late times. Furthermore, the factor C_M depends on the Lundquist number, but is expected to reach an asymptotic value of about 50 [29]. The correct prefactors in the scaling relations (30) and (32) depend on which conserved quantity governs the decay. When the decay is governed by $I_H = $ const, we have

$$k_i = C_k^H I_H^{-1/9}\tau_i^{-4/9}, \qquad B_i = C_B^H I_H^{1/9}\tau_i^{-5/9}, \tag{51}$$

while when the decay is governed by $I_M = $ const, we have

$$k_i = C_k^M I_M^{-1/3}\tau_i^{-2/3}, \qquad B_i = C_B^M I_M^{1/3}\tau_i^{-1/3}. \tag{52}$$

Here, the subscript i refers to the points A or B, or to any other moment in time. The values of the prefactors C_k^H, C_B^H, C_k^M, and C_B^M are still somewhat uncertain, but it is suspected that they are universal. Furthermore, they were given in terms of length scales and energy densities. See Table I for a comparison showing that different measurements resulted in similar values.

TABLE I. Comparison of the prefactors C_k^H, C_k^M, C_B^H, and C_B^M found in earlier work.

Prefactor	[31]	[25]	[32]	
$C_k^H = 1/C_\xi^H$	1/0.15	1/0.12	1/0.14	≈7.1
$C_k^M = 1/C_\xi^M$	⋯	⋯	1/0.12	≈8.3
$C_B^H = \sqrt{2C_\mathcal{E}^H}$	$\sqrt{2\times 3.8}$	$\sqrt{2\times 3.7}$	$\sqrt{2\times 4.0}$	≈2.8
$C_B^M = \sqrt{2C_\mathcal{E}^M}$	⋯	⋯	$\sqrt{2\times 4.0}$	≈2.8

The quantities I_H and I_M can be approximated in terms of their dimensions, as has been done previously [22,32]. Here, the magnetic field is always understood as being expressed as an Alfvén velocity. It is then possible to cast Eqs. (51) and (52) in terms of $k_A(\tau_{\rm EW})$ and $B_A(\tau_{\rm EW})$. However, given that the original expressions are based on potentially universal prefactors and on conserved quantities that can, in principle, be accurately determined, it is clear that the expressions (30) and (32) cannot be applied to arbitrarily chosen starting values.

VI. CONCLUSIONS

We have shown that arguments based on symmetries of the electroweak vacuum manifold imply the production of magnetic fields that are largely independent of the details of the symmetry breaking process. We have used these arguments to evaluate the energy spectrum of the magnetic field and find $E_M \propto k^4$ on large length scales (small k). Without CP violation in the model, the average magnetic helicity vanished, but there were helicity fluctuations on all scales. Together with earlier results from field theory simulations of electroweak symmetry breaking and MHD simulations of cosmological magnetic field evolution, we have estimated the magnetic field strength and coherence scale at the present epoch. For nonhelical fields, we found kpc coherence scales and 10^{-13} G field strength, while for maximally helical fields, we found Mpc coherence scales and 10^{-10} G field strength. For fractional helicity, the estimates were between these extreme values. Such estimates are consistent with current upper and lower bounds on cosmological magnetic fields [7,9].

An important assumption in these estimates is that the initial coherence scale of the magnetic field is given by the horizon size at the electroweak epoch. There is some supporting numerical evidence from field theory simulations that show that the spectrum is peaked at the largest length scales in the simulations [2–4]. It would be reassuring to see the result hold up in bigger simulation volumes.

If the initial coherence scale is subhorizon, the subhorizon dynamics should be taken into account and the estimates should be rescaled accordingly.

The limitations of our analysis should be pointed out. The nondynamical algorithm of Sec. IV is suitable for determining properties of the magnetic field that are insensitive to the symmetry breaking dynamics. For example, the method can give us the spectrum k^4 but it cannot give us the coherence scale of the magnetic field, which depends on the evolution during the symmetry breaking process. The coherence scale may also evolve with time, while the present algorithm is static and can at best provide a snapshot of the evolution. Lastly, we have ignored the contribution of the $\mathcal{A}$ term in (1), whereas the full dynamics of electroweak symmetry breaking will include all contributions.

ACKNOWLEDGMENTS

T. V. is grateful to Antonino Midiri and Teerthal Patel for discussions and to Chiara Caprini, Ruth Durrer, and Alberto Roper Pol for motivating the present analysis. We thank the Bernoulli Center, EPFL, Lausanne, for hospitality during the "Generation, Evolution, and Observations of Cosmological Magnetic Fields" workshop. T. V. thanks Tufts Institute of Cosmology for hospitality while this work was being done. This work was supported by the U.S. Department of Energy, Office of High Energy Physics, under Award No. DE-SC0019470. A. B. was supported in part by the Swedish Research Council (Vetenskapsrådet) under Grant No. 2019-04234, the National Science Foundation under Grant Nos. NSF PHY-2309135 and AST-2307698, and the NASA ATP Grant 80NSSC22K0825. We acknowledge the allocation of computing resources provided by the Swedish National Allocations Committee at the Center for Parallel Computers at the Royal Institute of Technology in Stockholm.

DATA AVAILABILITY

The source code used for the simulations of this study, the Pencil Code, is freely available from Ref. [15]. The simulation setups and data that support the findings of this article are openly available [33].

APPENDIX A: ANOTHER ALGORITHM

Once we have the Higgs distribution, we can calculate the gauge field using (7). The gauge fields are defined on the links of the lattice, and we will only need the component of the gauge field along the link. From (7) and (12) it follows that

$$\mathbf{A} = \frac{2\sin\theta_w}{g\eta^2}[\cos^2\alpha\nabla\beta + \sin^2\alpha\nabla\gamma]. \tag{A1}$$

Then $\mathbf{A}$ on a link is related to the Hopf angles at the end points of the link. As an example, consider the link from point (i,j,k) on the lattice to the point $(i+1,j,k)$. We first need to evaluate α at the central point $(i+1/2,j,k)$. This is done using

$$\Phi(i+1/2,j,k) = \frac{\Phi(i,j,k)+\Phi(i+1,j,k)}{|\Phi(i,j,k)+\Phi(i+1,j,k)|} \tag{A2}$$

and then

$$\cos\alpha = |\Phi_1(i+1/2,j,k)|, \qquad \sin\alpha = |\Phi_2(i+1/2,j,k)|, \tag{A3}$$

where the subscripts 1 and 2 on Φ denote its upper and lower components. Calculating the gradients of β and γ in (A1) requires some care since the angles are defined on a circle. For example,

$$\nabla_x\beta(i+1/2,j,k) = [[\beta(i+1,j,k)-\beta(i,j,k)]]/\delta x, \tag{A4}$$

where $[[\cdot]]$ means that the difference is taken to lie in the interval $[-\pi,\pi]$. Operationally, if the difference $\beta(i+1,j,k)-\beta(i,j,k)$ is larger than π, then we subtract 2π, and if it is smaller than $-\pi$, we add 2π. We have tested this algorithm for Φ_m given by (8) and found excellent agreement with the analytical result in (11), even for relatively coarse lattices. However, we observe no significant difference in the spectral properties of the magnetic field by using this method.

APPENDIX B: ANALYTICAL REASONING

In Ref. [9], an analytical argument was used to derive the energy spectrum of the magnetic field resulting from electroweak symmetry breaking. The conclusion was a k^3 spectrum. In this appendix we revisit the argument, identify an error, and correct it to obtain a spectrum consistent with our numerical results.

We consider the volume-averaged magnetic field vector, defined as

$$B_{V,i} = \frac{1}{V}\int_V d^3x\, B_i(\mathbf{x}), \tag{B1}$$

where V is the averaging volume. On average, $B_{V,i}$ vanishes owing to isotropy. However, the variance of $B_{V,i}$ does not vanish,

$$B_V \equiv \langle \mathbf{B}_V^2\rangle^{1/2} = \left\langle \left(\frac{1}{V}\int_V d^3x\mathbf{B}(\mathbf{x})\right)^2\right\rangle^{1/2}, \tag{B2}$$

where $\langle\cdot\rangle$ denotes ensemble averaging.

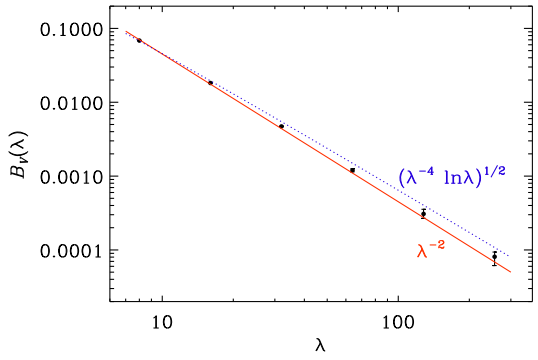

FIG. 6. Log-log plot of volume-averaged magnetic field, B_V, versus size of volume, shown as black dots. The error bars have been computed based on averaging over the three coordinate directions of the magnetic field. The red line has a slope of -2 and the blue dotted line shows $(\lambda^{-4}\ln\lambda)^{1/2}$.

To estimate B_V, we use Eq. (6),

$$\frac{1}{V}\int_V d^3x B_i(\mathbf{x}) = -i\frac{2\sin\theta_w}{g\eta^2 V}\int_V d^3x \epsilon_{ijk}\partial_j\Phi^\dagger\partial_k\Phi = -i\frac{2\sin\theta_w}{g\eta^2 V}\int_{\partial V} dS^j \epsilon_{ijk}\Phi^\dagger\partial_k\Phi, \tag{B3}$$

where ∂V is the boundary of the volume V. The Higgs field magnitude is fixed to be the VEV, denoted by η, and so the gradients of Φ are of order η/d, where d is the domain size over which Φ is approximately constant. Then the integral is a sum of terms of magnitude $\sim\eta^2/d$ but with random signs. If $V=\lambda^3$, the number of independent terms in the integral is λ^2/d^2 and, as for a random walk, the integral grows with λ as $\sqrt{\lambda^2/d^2}\propto\lambda$. The prefactor scales as $1/V=1/\lambda^3$, implying that B_V scales as $1/\lambda^2$, and hence

$$B_V \propto \frac{1}{\lambda^2}\propto k^2. \tag{B4}$$

This scaling is confirmed by our numerical analysis and is shown in Fig. 6.

The next step is to connect B_V to the energy spectrum $E_M(k)$. The connection is [9]

$$B_V^2 = 2\int dk\, E_M(k) W_V^2(k), \tag{B5}$$

where the window function $W_V(k)$ is defined as

$$W_V(k) = 3j_1(k\lambda)/(k\lambda), \tag{B6}$$

where $j_1(x)=(\sin x - x\cos x)/x^2$ is the spherical Bessel function.

In Ref. [9] it was estimated that $B_V^2\sim kE_M(k)$, but this is not correct, as we now see. Let us consider power law forms of $E_M(k)$ with a cutoff at k_*,

$$E_M(k) = \begin{cases} Ak^n, & k\le k_* \\ 0, & k>k_* \end{cases}. \tag{B7}$$

Then (B5) can be written as

$$B_V^2 = \frac{2A}{\lambda^{n+1}}\int_0^{K_*} dq q^n \left[\frac{3}{q^3}(\sin q - q\cos q)\right]^2, \tag{B8}$$

where $K_*\equiv k_*\lambda\gg 1$ because we are interested in the magnetic field on large length scales. For $n\ge 3$, the integral is dominated by the upper limit, where $q\gg 1$. Then we can estimate

$$B_V^2 \sim \frac{9A}{\lambda^{n+1}}\int^{K_*} dq\, q^{n-4} \propto \begin{cases} \lambda^{-4}\ln\lambda, & n=3 \\ \lambda^{-4}, & n\ge 4 \end{cases}. \tag{B9}$$

Since (B4) tells us that $B_V^2\sim k^4\sim\lambda^{-4}$, we must have $E_M(k)\propto k^n$ for $n\ge 4$. In particular, $E_M(k)\propto k^3$ does not follow.

Note that $E_M\propto k^4$ is consistent with the claim in Ref. [34] even though our reasoning is nondynamical and causality considerations are not relevant.

APPENDIX C: RELATION TO EARLIER USED EXPONENTS

To facilitate the comparison between the scaling exponents used here and those used in earlier papers, we list in Table II the most important ones. We also list their values that are relevant when the MHD decay is governed either by $I_H=$ const or by $I_M=$ const.

The scaling exponent $2/(\epsilon+3)$ in Eq. (28) characterizes the growth of the characteristic length scale with time and was denoted in Ref. [26] by q. The scaling of the magnetic field with the characteristic length scale was denoted in Ref. [29] by κ and is related to the exponent $p=(\epsilon+1)/(\epsilon+3)$ introduced in Eq. (32), such that $p=\kappa q$. The exponent $\gamma=2(s-\epsilon)/(\epsilon+3)$ in Eq. (27) agrees with the expression $(\alpha-\beta)q$ in Eq. (2.9) of Ref. [25].

The observation that the exponents p and $2/(\epsilon+3)$ add up to unity reflects the fact that the Alfvén time is proportional to the actual (conformal) time τ. This is true regardless of whether the MHD decay is governed by $I_H=$ const or by $I_M=$ const.

TABLE II. Relation between the scaling exponents used here and those used in earlier literature, along with their values when the MHD decay is governed either by $I_H=$ const or by $I_M=$ const.

Present work	Earlier work	$I_H=$ const	$I_M=$ const
s	α [26,35]	Arbitrary	
ϵ	β [26]	3/2	0
$2/(\epsilon+3)$	q [26]	4/9	2/3
p	$q\kappa$ [29]	5/9	1/3

[1] T. Vachaspati, Magnetic fields from cosmological phase transitions, Phys. Lett. B **265**, 258 (1991).

[2] A. Diaz-Gil, J. Garcia-Bellido, M. Garcia Perez, and A. Gonzalez-Arroyo, Magnetic field production during preheating at the electroweak scale, Phys. Rev. Lett. **100**, 241301 (2008).

[3] A. Diaz-Gil, J. Garcia-Bellido, M. Garcia Perez, and A. Gonzalez-Arroyo, Primordial magnetic fields from preheating at the electroweak scale, J. High Energy Phys. 07 (2008) 043.

[4] Y. Zhang, T. Vachaspati, and F. Ferrer, Magnetic field production at a first-order electroweak phase transition, Phys. Rev. D **100**, 083006 (2019).

[5] D. Grasso and H. R. Rubinstein, Magnetic fields in the early universe, Phys. Rep. **348**, 163 (2001).

[6] L. M. Widrow, Origin of galactic and extragalactic magnetic fields, Rev. Mod. Phys. **74**, 775 (2002).

[7] R. Durrer and A. Neronov, Cosmological magnetic fields: Their generation, evolution and observation, Astron. Astrophys. Rev. **21**, 62 (2013).

[8] K. Subramanian, The origin, evolution and signatures of primordial magnetic fields, Rep. Prog. Phys. **79**, 076901 (2016).

[9] T. Vachaspati, Progress on cosmological magnetic fields, Rep. Prog. Phys. **84**, 074901 (2021).

[10] T. W. B. Kibble, Topology of cosmic domains and strings, J. Phys. A **9**, 1387 (1976).

[11] A. Vilenkin and E. P. S. Shellard, *Cosmic Strings and Other Topological Defects* (Cambridge University Press, Cambridge, England, 2000).

[12] Y. Nambu, String-like configurations in the Weinberg-Salam theory, Nucl. Phys. **B130**, 505 (1977).

[13] T. Patel and T. Vachaspati, Kibble mechanism for electroweak magnetic monopoles and magnetic fields, J. High Energy Phys. 01 (2022) 059.

[14] T. Patel and T. Vachaspati, Annihilation of electroweak dumbbells, J. High Energy Phys. 02 (2024) 164.

[15] A. Brandenburg *et al.* (Pencil Code Collaboration), The Pencil Code, a modular MPI code for partial differential equations and particles: Multipurpose and multiuser-maintained, J. Open Source Software **6**, 2807 (2021).

[16] G. W. Gibbons, M. E. Ortiz, F. Ruiz Ruiz, and T. M. Samols, Semilocal strings and monopoles, Nucl. Phys. **B385**, 127 (1992).

[17] G. 't Hooft, Magnetic monopoles in unified gauge theories, Nucl. Phys. **B79**, 276 (1974).

[18] A. M. Polyakov, Particle spectrum in quantum field theory, JETP Lett. **20**, 194 (1974).

[19] A. Achucarro and T. Vachaspati, Semilocal and electroweak strings, Phys. Rep. **327**, 347 (2000).

[20] D. N. Hosking and A. A. Schekochihin, Reconnection-controlled decay of magnetohydrodynamic turbulence and the role of invariants, Phys. Rev. X **11**, 041005 (2021).

[21] D. N. Hosking and A. A. Schekochihin, Cosmic-void observations reconciled with primordial magnetogenesis, Nat. Commun. **14**, 7523 (2023).

[22] H. Zhou, R. Sharma, and A. Brandenburg, Scaling of the Hosking integral in decaying magnetically dominated turbulence, J. Plasma Phys. **88**, 905880602 (2022).

[23] T. Vachaspati, Estimate of the primordial magnetic field helicity, Phys. Rev. Lett. **87**, 251302 (2001).

[24] A. Brandenburg and T. Kahniashvili, Classes of hydrodynamic and magnetohydrodynamic turbulent decay, Phys. Rev. Lett. **118**, 055102 (2017).

[25] A. Brandenburg, R. Sharma, and T. Vachaspati, Inverse cascading for initial magnetohydrodynamic turbulence spectra between Saffman and Batchelor, J. Plasma Phys. **89**, 905890606 (2023).

[26] A. Brandenburg, T. Kahniashvili, S. Mandal, A. Roper Pol, A. G. Tevzadze, and T. Vachaspati, Evolution of hydromagnetic turbulence from the electroweak phase transition, Phys. Rev. D **96**, 123528 (2017).

[27] J. M. Cornwall, Speculations on primordial magnetic helicity, Phys. Rev. D **56**, 6146 (1997).

[28] T. Vachaspati and A. Vilenkin, Cosmological chirality and magnetic fields from parity violating particle decays, Phys. Rev. D **103**, 103528 (2021).

[29] A. Brandenburg, A. Neronov, and F. Vazza, Resistively controlled primordial magnetic turbulence decay, Astron. Astrophys. **687**, A186 (2024).

[30] R. Banerjee and K. Jedamzik, Evolution of cosmic magnetic fields: From the very early Universe, to recombination, to the present, Phys. Rev. D **70**, 123003 (2004).

[31] A. Brandenburg and G. Larsson, Turbulence with magnetic helicity that is absent on average, Atmosphere **14**, 932 (2023).

[32] A. Brandenburg and A. Banerjee, Turbulent magnetic decay controlled by two conserved quantities, J. Plasma Phys. **91**, E5 (2025).

[33] T. Vachaspati and A. Brandenburg, Datasets of spectra of magnetic fields from electroweak symmetry breaking, Zenodo 14796972 (v2025.01.03), 10.5281/zenodo.14796972 (2025); See also http://norlx65.nordita.org/~brandenb/proj/EW-B-statistics/.

[34] R. Durrer and C. Caprini, Primordial magnetic fields and causality, J. Cosmol. Astropart. Phys. 11 (2003) 010.

[35] P. Olesen, Inverse cascades and primordial magnetic fields, Phys. Lett. B **398**, 321 (1997).